Toward Optimal Conjunction-Based Sensor Tasking using Inferential Moments

Dr. Kevin Vanslette
Raytheon BBN
Roddy Taing
University of Wisconsin-Madison

ABSTRACT

We provide a framework for the automatic refining and tracking of conjunction probability estimates, which we call conjunction-based sensor tasking. This differs from traditional custody-based sensor tasking which instead refines resident space object coordinate uncertainties. Our algorithm utilizes inferential variance [1] as its objective function, which ranks conjunction scenarios by the amount their conjunction probabilities are expected to deviate in response to measurement. We simulate many conjunction sensor tasking scenarios and demonstrate that our approach is more effective at refining conjunction probabilities in terms of mean square error than information theoretic methods and seemingly reasonable "rule-of-thumb" methods that are perhaps in use today. We also present two secondary results: The first is a theoretical extension of the inferential moment approach to custody-based sensor tasking, for completeness. The second involves characterizing a few aspects of the optimal custody and conjunction-based sensor tasking problems at hand. We prove in general that the inferential variance is non-decreasing and supermodular under the addition of more sensors. In addition, we prove that the Mutual Information is non-decreasing and supermodular given that all the sensors are conditionally independent from one another, which is an assumption that aligns with the Kalman Filter paradigm for custody-based sensor tasking. Some approximate polynomial complexity algorithms exist for this class of size constrained, non-decreasing, supermodular NP-hard optimization problems, which we hope to explore in future work.

1. INTRODUCTION

The problem of custody-based sensor tasking and tracking for Space Domain Awareness (SDA) has been studied extensively in the literature. Due to the presence of process noise in the Kalman Filter paradigm or the possibility of an unscheduled maneuver, the position-velocity state uncertainties of Resident Space Objects (RSOs) tend to grow with time; however, by making measurements with sensors, these uncertainties may be kept in check [2, 3, 4, 5, 6, 7]. Keeping custody of RSOs enables more accurate reasoning and situational SDA, for instance, by enabling more informed computation of future events like conjunctions.

Because sensing resources are finite and imperfect, not every space object can be tracked with certainty at all times; thus, sensor tasking optimization schemes are developed to make the most of finite resources. Mutual Information (MI), Information Gain (IG), and the trace of the Fisher Information Matrix (FIM) are often used as objective functions for optimizing custody-based sensor tasking schedules. Traditional optimization schemes have been applied to the problem of optimized sensor tasking schedules [2, 3, 5, 6] as well as newer-age reinforcement learning schemes like [8]. By choosing optimal schedules according to information-based objective functions, one seeks solutions that reduce track uncertainty in an informational sense.

A recent article, "Inferential Moments of Uncertain Multivariable Systems" [1], defines a new set of quantities called "inferential moments" that can be used for optimal sensor tasking. Inferential moments are formulated from Bayes Rule updating. According to Bayes Rule, the probability of an occurrence $a \in A$,

$$p(a) \xrightarrow{B} p(a|b), \tag{1}$$

is updated from its prior value $p(a)$ to a posterior value $p(a|b)$ given a new measured (or learned old) value $b \in B$. However, prior to measurement, the true value of B is unknown and is distributed according to $p(b)$. Thus it is

uncertain as to which value the prior probability $p(a)$ will update to... will $p(a)$ update to $p(a|b)$ or to some other probability value, e.g. $p(a|b') \neq p(a|b)$? From this perspective, $p(a|b)$ itself may be treated as a random variable and inferential moments capture the statistical moments corresponding to this randomness. The first inferential moment corresponds to the equation for a (marginal) prior probability distribution, which in this context is understood to be the expected value of the conditional probability $p(a) = E_B[p(a|b)] = \sum_{b\in B} p(b)p(a|b)$. Higher order inferential moments $E_B[p(a|b)^n]$ quantify behavioral information about how the distribution is expected to respond to new information. In particular, the second-order central inferential moment, the inferential variance,

$$\mathrm{Var}_B\Big[p(a|b)\Big] = \sigma_B^2[p(a|b)] = \mathrm{E}_B\Big[(p(a|b) - p(a))^2\Big] = \sum_{b\in B} p(a|b)^2 p(b) - p(a)^2, \tag{2}$$

quantifies how much the probability $p(a)$ is expected to fluctuate due to the utilization of a measurement device B. Variation of this type is shown in Fig. 1.

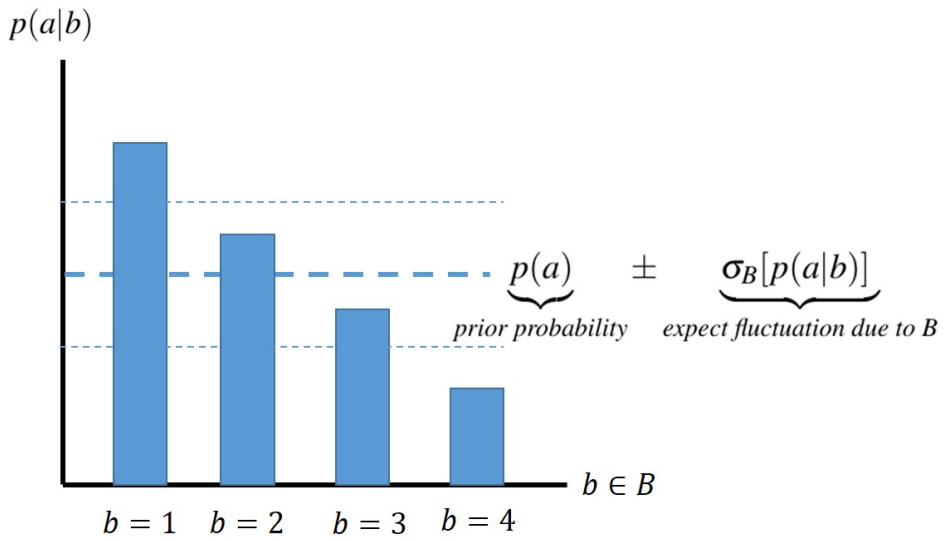

Fig. 1: The inferential variance of $p(a)$ due to an unknown or random, but conditionally dependent, measurable variable $b \in B$.

Reference [1] finds an expansion of the Mutual Information in terms of inferential moments, which indicates that inferential moments are quantities that may be able to help with tasks normally tackled with information theoretic quantities, e.g. optimal sensor tasking. The inferential variance of $p(a)$ due to a measurement B can be interpreted as an unbiased Mean Squared Error (MSE) between $p(a|b)$ and $p(a)$,

$$\mathrm{Var}_B\Big[p(a|b)\Big] = \mathrm{E}_B\left[\Big(p(a|b) - \mathrm{E}_B\Big[p(a|b)\Big]\Big)^2\right] = \mathrm{E}_B\Big[(p(a|b) - p(a))^2\Big] = \mathrm{MSE}\Big(p(a|b), p(a)\Big), \tag{3}$$

thus the inferential variance can also be interpreted as the expected square error of probability incurred by using $p(a)$ to estimate the random variable $p(a|b)$ (as shown in Fig. 1). This is a helpful notion as it provides a direct quantitative, error-based, interpretation of the "goodness of fit" gained by making a measurement as compared to quantities like the "amount of information gained", which is a quantity typically only understood by experts or understood in ratio to other amounts of information. Thus, ranking sensors according to which sensor yields the largest inferential variance provides a error-centric, rather than information-centric, objective function for sensor tasking.

We develop two optimal sensor tasking objectives using inferential moments in this article. The first objective is the traditional objective of maintaining accurate position-velocity tracks of RSOs, e.g. custody-based tracking. Because the FIM is a measure of local MI and because the MI is the unique functional for quantifying global (linear or non-linear) correlations between pairs of variables [9, 10], it is suspected that the MI is a superior objective function for custody-based sensor tasking than the FIM [6, 11]. Recently, [6] performed an in-depth analysis using the Mutual

Information as an objective function for dynamic custody-based sensor tasking of UAVs and satellites. They proposed several greedy approaches to approximate the NP-hard optimal solution by maximizing MI sequentially in time, sensors, and/or RSOs. For linearly correlated (Gaussian) variables in the Kalman Filter paradigm, we find similarities between the exhaustive inferential variance objective function and the Mutual Information: both lead to the same custody-based sensor tasking ranking scheme for single RSOs due to being monotonic in the same decision variables and both are non-decreasing and supermodular (contrary to [6] which claims submodularity and which differs from the conclusions under related conditions from [12, 13]). The maximization of a size-constrained, supermodular, objective function is an NP-hard optimization problem with limited guarantees (i.e. there is no $\frac{e-1}{e}$ greedy algorithm performance guarantee as there is for constrained, non-decreasing submodular functions). This class of optimization problem is still under investigation in the literature, but progress has been made recently resulting in an algorithm that computes a portion of the exact solutions in polynomial time using minimum norm base [14], which may be sufficient for this problem.

The second sensor tasking objective we consider optimizes sensor tasking for refining and more accurately tracking conjunction probability estimates, which we call "conjunction-based" sensor tasking. In contrast to custody-based sensor tasking, which is optimized toward maximally reducing position-velocity RSO state uncertainties, we seek a sensor tasking ranking scheme that provides the most valuable knowledge towards updating and refining conjunction probabilities themselves.

Reference [15] outlines the state of the art and future needs in Conjunction Analysis (CA). CA is broken into four stages (paraphrased here):

(CA 1) Screening for potential conjunctions

(CA 2) Conjunction risk probability computation

(CA 3) Refinement of risk using updated orbital data from measurements

(CA 4) Conjunction avoidance action

Our aim is to formalize stage CA 3. The authors are not aware of formalized approaches for studying something like "conjunction-based" sensor tasking outside of rule-of-thumb approaches such as tasking by the largest: conjunction probability, covariance, asset value, etc. The primary outcome of this article is the formulation and demonstration of a conjunction-based sensor tasking objective function that yields better conjunction probability estimates in terms of mean squared error over information theoretic and rule-of-thumb based methods, which we simulate over a large variety of scenarios.

Because operators typically have two options for evaluating a potential conjunction event – Probability of Collision (PoC) or exclusion volume – we evaluate conjunction-based sensor tasking over a large range of exclusion volumes from ones that tightly couple collision radii to exclusion volumes that may be much larger than current positional covariances. An interesting observation about the latter is that more probability can be gained/lost at the boundary of the exclusion volume than in the center, which implies "nearest approach" conjunction probability schemes may be insufficient for some conjunction-based sensor tasking scenarios. To not introduce unnecessary complication into our simulation and to keep the analysis generally applicable in a variety of space domains and orbital volumes, we did not simulate full orbital propagation and full dynamic sensor tasking. We instead focused on varying a large number of representative conjunction scenarios near and through the boundary with simple dynamics to explore how different methods rank the value of tasking sensors in these scenarios.

2. THEORY

We use a looser definition of "conjunction" than is common in the literature. Because we will always define a conjunction boundary with some inter-RSO distance, we let "conjunction" mean either a physical collision (when the boundary is very small) or an exclusion zone (when the boundary is large).

We will first describe how traditional custody-based sensor tasking can be done using inferential moments and compare it functionally with the Mutual Information. We then introduce and discuss some potential rule-of-thumb approaches for conjunction-based sensor tasking before formulating optimal conjunction-based sensor tasking using inferential moments.

2.1 Custody-Based Sensor Tasking with Inferential Moments

The aim of custody-based sensor tasking is to best track the multidimensional coordinates of an RSO of interest $x \in X$ using the continuous multidimensional measurement variables of a sensor $y \in Y$. Optimal sensor tasking involves the selection of which sensors $Y \to \mathbb{Y} = \{Y^{(k)}\}$ of a set of K sensors to task to measure which RSOs $X \to \mathbb{X} = \{X^{(m)}\}$ of a set of M RSOs such that an objective function $J[\mathbb{X}, \mathbb{Y}, \Theta]$ is optimized. We seek a sensor configuration $\Theta = \{\theta^{(m,k)}\}$, where each decision variable $\theta^{(m,k)} \in \{0,1\}$ represents the tasking of the kth sensor to the mth entity, subject to sensor availability $\sum_k \theta^{(m,k)} \leq K$ (this constraint may be modified if a sensor can be tasked to simultaneously view multiple RSOs). Thus, optimal custody-based sensor tasking is a constrained nonlinear binary-integer programming (optimization) problem [6]:

$$\underset{\{\theta^{(m,k)}\}}{\arg\max}\, J[\mathbb{X}, \mathbb{Y}, \Theta] \;\text{ s.t. }\; \sum_{m,k} \theta^{(m,k)} \leq K. \tag{4}$$

This can be expanded to a dynamic optimal sensor tasking framework with a finite time horizon of τ simply by expanding the entity variables $X^{(m)} \to X^{(m)}_{0:\tau} \equiv \prod_{t=0}^{\tau} X^{(m)}_t = X^{(m)}_0 \times X^{(m)}_1 \times ... \times X^{(m)}_\tau$ over τ and similarly expanding $Y^{(k)} \to Y^{(k)}_{0:\tau}$ and $\Theta \to \Theta_{0:\tau}$. Given $J[\mathbb{X}, \mathbb{Y}, \Theta]$ is non-decreasing, and due to the size constraint, this class of sensor tasking algorithms is known to be NP-hard.

We explore custody-based sensor tasking with inferential moments. In the continuous domain, the inferential variance is,

$$\mathrm{Var}_Y\Big[\rho(x|y)\Big] = \mathrm{E}_Y\left[\Big(\rho(x|y) - \rho(x)\Big)^2\right] \equiv \sigma^2_Y\Big[\rho(x|y)\Big], \tag{5}$$

which is an expression of how much the uncertainty of a continuous state variable x, described by the probability density $\rho(x)$, is expected to vary in response to an uncertain measurement variable y. We quantify the point to point effect of a measurement over the entire domain of X using the "exhaustive inferential variance".

$$\triangle^2(X)_Y \equiv \int_{x \in X} \mathrm{Var}_Y\Big[\rho(x|y)\Big]\, dx \geq 0, \tag{6}$$

which is a "sum of squares". It may be interesting to note that $\mathrm{Var}_Y\left[\int_{x\in X} \rho(x|y)\, dx\right] = \mathrm{Var}_Y\Big[1\Big] = 0$ due to normalization.

Because multiple sensors may be tasked to measure the same entity m, let $\mathbb{Y}^{(m)} \equiv \prod_{k \in \boldsymbol{\kappa}^{(m)}} Y^{(k)} \subseteq \mathbb{Y}$ be the Cartesian product of the set of sensors tasked to measure m, $\mathbf{y}^{(m)} \in \mathbb{Y}^{(m)}$ be a coordinate of $\mathbb{Y}^{(m)}$, and $\boldsymbol{\kappa}^{(m)}$ be the set of k's that have been tasked to m (i.e. the set of k's for which $\theta^{(m,k)} = 1$). In this notation, the exhaustive inferential variance is

$$\triangle^2(X^{(m)})_{\mathbb{Y}^{(m)}} \equiv \int_{x^{(m)} \in X^{(m)}} \mathrm{Var}_{\mathbb{Y}^{(m)}}\Big[\rho(x^{(m)}|\mathbf{y}^{(m)})\Big]\, dx^{(m)}. \tag{7}$$

Given M independent entities and K sensors, we propose the following custody-based sensor tasking optimization using inferential moments,

$$\underset{\{\theta^{(m,k)}\}}{\arg\max} \left(\sum_m \triangle^2(X^{(m)})_{\mathbb{Y}^{(m)}}\right) \;\text{ s.t. }\; \sum_{m,k} \theta^{(m,k)} \leq K. \tag{8}$$

Due to the MSE-to-inferential variance relationship in (3), tasking sensors such that this quantity is maximized aims to produce an updated probability state that has removed the maximum amount of MSE between its current prior estimate of the distribution and its set of possible posterior distributions had the RSO been fully measured, following [1].

The Kalman Filter paradigm can be characterized as the propagation and measurement updating of multivariate Gaussian distributed variables (for review see [6, 16]). Let the pair of coordinates $(x,y) \equiv z$ be distributed according to $z \sim N\Big(\mu_Z, \Sigma_Z\Big)$, which is a $k_Z = k_X + k_Y$ dimensional multivariate Gaussian with parameters $\mu_Z = (\mu_X, \mu_Y)$ and $\Sigma_Z = \begin{bmatrix}\Sigma_X, \Sigma_{XY} \\ \Sigma^T_{XY}, \Sigma_Y\end{bmatrix}$. We are interested in the inferential variances of x's given measurements of y's. The conditional multivariate Gaussian is,

$$\rho(x|y) = N\Big(\mu'_X(y), \Sigma'_X\Big) \equiv N\Big(\mu_X + \Sigma_{XY}\Sigma_Y^{-1}(y - \mu_Y), \Sigma_X - \Sigma^T_{XY}\Sigma_Y^{-1}\Sigma_{XY}\Big), \tag{9}$$

and the relevant marginal distributions are $\rho(y) = N\Big(\mu_Y, \Sigma_Y\Big)$ and $\rho(x) = N\Big(\mu_X, \Sigma_X\Big)$. The computation of the exhaustive inferential variance for this case is in Appendix 7.1, the result of which is

$$\begin{aligned} \triangle^2(X)_Y &= \int_{x,y\in X,Y} N\Big(\mu'_X(y), \Sigma'_X\Big)^2 \rho(y)\, dy\, dx - \int_{x\in X} N\Big(\mu_X, \Sigma_X\Big)^2 dx \\ &= \frac{1}{\sqrt{2}(2\pi)^{k_X/2}}\Big(\frac{1}{|\Sigma'_X|^{\frac{1}{2}}} - \frac{1}{|\Sigma_X|^{\frac{1}{2}}}\Big). \end{aligned} \tag{10}$$

Note that because Σ_X is the prior covariance of the physical variables of interest, it is constant under a change of measurement device $Y^{(k)} \to Y^{(k')}$, while $\Sigma'_X = \Sigma_X - \Sigma_{XY}^T \Sigma_Y^{-1} \Sigma_{XY}$ is not. Further note that $\triangle(X)_Y$ is a monotonic function of $|\Sigma'_X|$.

Similarly, the Mutual Information between X and Y is [6, 17],

$$\mathrm{MI}[X;Y] = \frac{1}{2}\ln\Big(\frac{|\Sigma_X|}{|\Sigma'_X|}\Big), \tag{11}$$

which is also monotonic in $|\Sigma'_X|$ and can be interpreted as the prior to posterior (post-measurement) covariance ratio. Because both the exhaustive inferential variance and MI are monotonic in $|\Sigma'_X|$, they necessarily achieve the same ranking for all sensor tasking combinations *for a single RSO*, i.e. when the $|\Sigma_X|$ term can effectively be ignored. However, if there are multiple RSOs, the tasking is different. As an example, consider that the MI of two different RSOs is equal if the ratio of their prior to posterior determinants is constant, i.e. $r = \frac{|\Sigma_X^{(1)}|}{|\Sigma_X'^{(1)}|} = \frac{|\Sigma_X^{(2)}|}{|\Sigma_X'^{(2)}|} \geq 1$ implies $\mathrm{MI}[X^{(1)};Y^{(k)}] = \mathrm{MI}[X^{(2)};Y^{(k')}] = \frac{1}{2}\ln\Big(r\Big)$. On the other hand, the exhaustive inferential variance does not have this property because $\triangle(X)_Y \propto \frac{r-1}{|\Sigma_X|}$. The exhaustive inferential variance is larger on a point-by-point basis over the probability density function for narrower Gaussian distributions (at least when determinant ratios are held constant).

In Appendix 7.2.1 we prove that the exhaustive inferential variance is non-decreasing and supermodular under the addition of more sensors and in Appendix 7.2.2 we similarly prove the MI is non-decreasing and supermodular, so there is no greedy algorithm efficiency guarantee as there would if it were submodular. This does not imply that simple approximate (or sometimes exact) algorithms cannot be found. Letting the generalization (8) to the dynamic optimal sensor tasking framework be summed over time,

$$\underset{\{\theta_t^{(m,k)}\}}{\arg\max} \left(\sum_{t=0}^{\tau} \sum_m \triangle^2(X_t^{(m)})_{\mathbb{Y}_{0:t}^{(m)}} \right) \text{ s.t. } \sum_{m,k} \theta_t^{(m,k)} \leq K, \ \forall t \in \tau, \tag{12}$$

the framework remains non-decreasing and supermodular. Due to the size constraints $\sum_{m,k} \theta_t^{(m,k)} \leq K$ and super modularity, this is a combinatorial NP-hard optimization problem with complexity $2^{M\times K\times\tau}$. Efficiency and computational complexity guarantees for approximate algorithms that solve this class of optimization problem are still under investigation in the literature, but progress has been made recently resulting in an algorithm that computes a portion of exact optimal solutions in polynomial time through minimum norm base [14]. More research and exploration is needed for this class of optimization problems in this setting. We shift to conjunction-based sensor tasking.

2.2 Conjunction-based Sensor Tasking with Rule-of-Thumb (RoT) Tasking

Once M RSOs have been identified as potentially being at risk for conjunction in CA 1 and a probability of conjunction $p(c^{(m,m')})$ is calculated in CA 2 (forward equation (13)), operators aim to refine conjunction risk by updating orbital data from measurements in CA 3. Imagine a scenario where an operator has a limited number of available sensors and must make choices about which sensors to task to which RSOs to improve conjunction awareness and SDA. One can imagine the use of the following RoT schemes to task sensors based on which RSO has (or would have) the:

(RoT 1) Max probability of conjunction at closest approach

(RoT 2) Min trace or determinant posterior covariance

(RoT 3) Max custody-based MI – Prior to posterior (post-measurement) covariance ratio, eq. (11)

(RoT 4) Max asset value – $\max\left(\left\{v^{(m)}+v^{(m')}\right\}\right)$

(RoT 5) Max expected asset risk value – $\max\left(\left\{(v^{(m)}+v^{(m')})p(c^{(m,m')})\right\}\right)$ [18]

At first glance, many of the items in the list seem reasonable – prioritize high probability conjunctions (RoT 1), reperform custody-based sensor tasking on the screened set (RoT 2, 3), or prioritize conjunction risk to high value assets (RoT 4, 5). Tasking based on any of those schemes would seemingly lead to a refinement of risk or the probability of a conjunction, but by how much? In an extreme scenario, imagine there is a 100% probability of conjunction. According to RoT 1, sensors would be tasked to measure RSOs from the 100% conjunction probability pair over any other conjunction pair; however, the probability of conjunction will remain at 100% post-measurement by definition – nothing about the probability of the conjunction was learned in the case where RoT 1 was supposed to be most effective.

The main point here is to emphasize that the overall objective of conjunction-based sensor tasking should be to *refine* risk assessment or conjunction probabilities, but the RoTs provided here are not optimizing some "amount of conjunction refinement", and thus they are bound to be suboptimal in some sense. RoT 2 and 3 aim to refine conjunction probabilities by refining custody-based state information. While custody-based state information is functionally related to the probability of a conjunction, optimizing for custody awareness does not guarantee optimizing for conjunction awareness. We will explore RoT 1, 2 and 3 in our conjunction-based sensor tasking simulation. RoT 4 is independent of conjunction and custody uncertainties, which is likely suboptimal when compared to RoT 5. It is worth emphasizing for RoT 5 that here we should be concerned with trying to *refine* the estimate of risk through sensor tasking, not reduce it by maneuvering, as we are concerned with CA 3 *not* CA 4; however, improving CA 3 can lead to more effective maneuvers in CA 4. We make some preliminary remarks about refining RoT 5 theoretically with inferential moments, but we believe more research is needed.

2.3 Conjunction-based Sensor Tasking with Inferential Moments

Let the conjunction boundary have radius $\mathscr{L}$. Given the positional probability distribution of two RSOs (for conjunction-based analysis let X be purely positional), both of which being independent multivariate Gaussian distributions, the probability of conjunction (i.e. they are within $\mathscr{L}$) is,

$$\begin{aligned} p(c^{(1,2)}) &\equiv p(c^{(1,2)}|\vec{\mu}_{L^{(1,2)}},\Sigma_{L^{(1,2)}}) \\ &= \frac{1}{(2\pi)^{k/2}|\Sigma_{L^{(1,2)}}|^{\frac{1}{2}}}\int_{\vec{L}^{(1,2)}}\mathbb{1}\left(L^{(1,2)}\leq\mathscr{L}\right)\exp\left(-\frac{1}{2}(\vec{L}^{(1,2)}-\vec{\mu}_{L^{(1,2)}})^T\Sigma^{-1}_{L^{(1,2)}}(\vec{L}^{(1,2)}-\vec{\mu}_{L^{(1,2)}})\right)d\vec{L}^{(1,2)} \\ &= E_{\vec{L}^{(1,2)}}\left[\mathbb{1}\left(L^{(1,2)}\leq\mathscr{L}\right)\right]\sim\frac{1}{N}\sum_{n=1}^{N}\mathbb{1}\left(L^{(1,2)}_{(n)}\leq\mathscr{L}\right)=\hat{p}(c^{(1,2)}). \end{aligned} \tag{13}$$

Here, $\mathbb{1}(...)\in\{0,1\}$ is the indicator function, $\vec{L}^{(1,2)}=\vec{x}^{(1)}-\vec{x}^{(2)}$ is the displacement vector, $L^{(1,2)}\equiv|\vec{L}^{(1,2)}|$, $\vec{\mu}_{L^{(1,2)}}=\vec{\mu}_{X^{(1)}}-\vec{\mu}_{X^{(2)}}$ is the miss distance, and $\Sigma_{L^{(1,2)}}\equiv\Sigma_{X^{(1)}}+\Sigma_{X^{(2)}}$ is the displacement covariance. The integral involved in computing $p(c^{(1,2)})$ is written as an expectation value of a binary variable, which can be estimated via Monte Carlo sampling (last line in (13)) – the estimation is unbiased and the variance of error of the estimation is simply $\sigma^2[\hat{p}(c^{(1,2)})]=p(c^{(1,2)})(1-p(c^{(1,2)}))/N$.

If a measurement is made of one of the RSOs using Y, the probability of conjunction is updated in (13),

$$p(c^{(1,2)}) \quad\xrightarrow{Y}\quad p(c^{(1,2)}|y)=p(c^{(1,2)}|\vec{\mu}'_{L^{(1,2)}}(y),\Sigma'_{L^{(1,2)}})\equiv p(c^{(1,2)}|\vec{\mu}'_{L^{(1,2)}},\Sigma'_{L^{(1,2)}}), \tag{14}$$

where it is understood that fusing this measurement using a Kalman Filter paradigm results in an update of $\vec{\mu}_{L^{(1,2)}}$ and $\Sigma_{L^{(1,2)}}$:

$$\begin{aligned} \vec{\mu}_{L^{(1,2)}} &\xrightarrow{Y} \vec{\mu}'_{L^{(1,2)}}(y)\equiv\vec{\mu}'_{L^{(1,2)}}, \\ \Sigma_{L^{(1,2)}} &\xrightarrow{Y} \Sigma'_{L^{(1,2)}}. \end{aligned} \tag{15}$$

Thus, prior to the measurement, one can consider the inferential variance of the conjunction probability due to a measurement from Y, which is,

$$\mathrm{Var}_Y\left[p(c^{(1,2)}|y)\right]=\mathrm{E}_Y\left[p(c^{(1,2)}|y)^2\right]-\mathrm{E}_Y\left[p(c^{(1,2)}|y)\right]^2=\int_{y\in Y}p(c^{(1,2)}|y)^2\rho(y)\,dy-p(c^{(1,2)})^2, \tag{16}$$

which again can be computed using Monte Carlo. Because the conjunction probability is a binary variable, the theoretical (yet unrealistic) maximum inferential deviation is $\sqrt{p(c^{(1,2)})(1-p(c^{(1,2)}))}$, which occurs if measurements of the system could determine the displacement vector $\vec{L}^{(1,2)}$ with complete certainty such that the updated probability of conjunction is 0 or 1. As we will compare this quantity to a conjunction-based Mutual Information, we note it for completeness,

$$\begin{aligned}\mathrm{MI}\Big[C^{(1,2)};Y\Big] &= \sum_{c^{(1,2)}\in C^{(1,2)}}\int_{y\in Y} p(c^{(1,2)}|y)\rho(y)\ln\Big(\frac{p(c^{(1,2)}|y)\rho(y)}{p(c^{(1,2)})\rho(y)}\Big)\,dy \\ &= \sum_{c^{(1,2)}\in C^{(1,2)}}\int_{y\in Y} p(c^{(1,2)}|y)\rho(y)\ln\Big(\frac{p(c^{(1,2)}|y)}{p(c^{(1,2)})}\Big)\,dy, \end{aligned} \tag{17}$$

which can be estimated using the same Monte Carlo estimated distributions as the inferential variance.

Because conjunction probability is normalized, $1 = p(c^{(1,2)}) + p(\bar{c}^{(1,2)})$, and the variable is binary, the exhaustive inverential variance,

$$\triangle^2(C^{(1,2)})_Y = \sum_{c^{(1,2)}\in C^{(1,2)}} \mathrm{Var}_Y\Big[p(c^{(1,2)}|y)\Big] = \mathrm{Var}_Y\Big[p(c^{(1,2)}|y)\Big] + \mathrm{Var}_Y\Big[1-p(c^{(1,2)}|y)\Big] = 2\,\mathrm{Var}_Y\Big[p(c^{(1,2)}|y)\Big],$$

is simply twice the inferential variance. Due to this, without loss of optimality, we write the dynamic sensor tasking problem for conjunction-based sensor tasking:

$$\underset{\{\theta_t^{(m,k)}\}}{\arg\max}\left(\sum_{t=0}^{\tau}\sum_{m>m'}^{M}\sum_{m'=1}^{M}\mathrm{Var}_{\mathbb{Y}_{0:t}^{(m)}\mathbb{Y}_{0:t}^{(m')}}\Big[p(c_t^{(m,m')}|\mathbf{y}_{0:t}^{(m)},\mathbf{y}_{0:t}^{(m')})\Big]\right)\ \text{s.t.}\ \sum_{m,k}\theta_t^{(m,k)} \le K,\ \forall t\in\tau, \tag{18}$$

Due to the result in Appendix 7.2.1, the objective function is non-decreasing and supermodular, and because it is constrained, the optimization problem is again NP-hard.

2.3.1 Risk and Asset Value Preliminary Remarks

We make some initial remarks about how conjunction-based tasking using inferential variance could help refine the expected risk profile, RoT 5. Let $R_t = R_t(\{v^{(m)}\})$ be the risk function at time t in terms of asset value (cost) $v^{(m)}$ [18]. The expected risk (e.g. loss of value) due to conjunctions at time t is,

$$\mathrm{E}_C[R_t] = \sum_{m>m'}^{M}\sum_{m'=1}^{M}(v^{(m)}+v^{(m')})p(c_t^{(m,m')}) \tag{19}$$

Given sensors are tasked up to time t, $\mathbb{Y}_{0:t}$, the posterior expected risk is the conditional risk of the measured values:

$$\mathrm{E}_C[R_t|\mathbf{y}_{0:t}] = \sum_{m>m'}^{M}\sum_{m'=1}^{M}(v^{(m)}+v^{(m')})p(c_t^{(m,m')}|\mathbf{y}_{0:t}^{(m)},\mathbf{y}_{0:t}^{(m')}). \tag{20}$$

From an inferential moment perspective, if $\mathbf{y}_{0:t}$'s are unknown, then $p(c_t^{(m,m')}|\mathbf{y}_{0:t}^{(m)},\mathbf{y}_{0:t}^{(m')})$'s are random variables and $(v^{(m)}+v^{(m')})$'s can be treated as constants. The variation of the expected conditional risk with respect to possible measurement outcomes (in the special case that RSOs are only involved in one conjunction at a time) is,

$$\begin{aligned}\mathrm{Var}_{\mathbb{Y}_{0:t}}\Big[\mathrm{E}_C[R_t|\mathbf{y}_{0:t}]\Big] &= \sum_{m>m'}^{M}\sum_{m'=1}^{M}\mathrm{Var}_{\mathbb{Y}_{0:t}^{(m)}\mathbb{Y}_{0:t}^{(m')}}\Big[(v^{(m)}+v^{(m')})p(c_t^{(m,m')}|\mathbf{y}_{0:t}^{(m)},\mathbf{y}_{0:t}^{(m')})\Big], \\ &= \sum_{m>m'}^{M}\sum_{m'=1}^{M}(v^{(m)}+v^{(m')})^2\,\mathrm{Var}_{\mathbb{Y}_{0:t}^{(m)}\mathbb{Y}_{0:t}^{(m')}}\Big[p(c_t^{(m,m')}|\mathbf{y}_{0:t}^{(m)},\mathbf{y}_{0:t}^{(m')})\Big] \end{aligned} \tag{21}$$

which is a reweighting of the objective function in (18). The standard deviation of the conditional expected risk is $\sqrt{\mathrm{Var}_{\mathbb{Y}_{0:t}}\Big[\mathrm{E}_C[R_t|\mathbf{y}_{0:t}]\Big]}$ and the standard deviation of an individual risk due to a particular measurement assignment

takes a natural form. It is the inferential deviation scaled by the risk value

$$(v^{(m)} + v^{(m')}) \cdot \sigma_{\mathbb{Y}_{0:t}^{(m)} \mathbb{Y}_{0:t}^{(m')}} \left[p(c_t^{(m,m')} | \mathbf{y}_{0:t}^{(m)}, \mathbf{y}_{0:t}^{(m')}) \right], \tag{22}$$

and so, the expected risk ,plus or minus the deviation of its risk due to measurement, is,

$$(v^{(m)} + v^{(m')}) \left(p(c_t^{(m,m')}) \pm \sigma_{\mathbb{Y}_{0:t}^{(m)} \mathbb{Y}_{0:t}^{(m')}} \left[p(c_t^{(m,m')} | \mathbf{y}_{0:t}^{(m)}, \mathbf{y}_{0:t}^{(m')}) \right] \right).$$

3. CONJUNCTION-BASED SENSOR TASKING SIMULATION AND RESULTS

We begin this section by gaining an intution for conjunction-based sensor tasking. Fig. 2 explores conjunction probability distributions and inferential variance in the large conjunction boundary case.

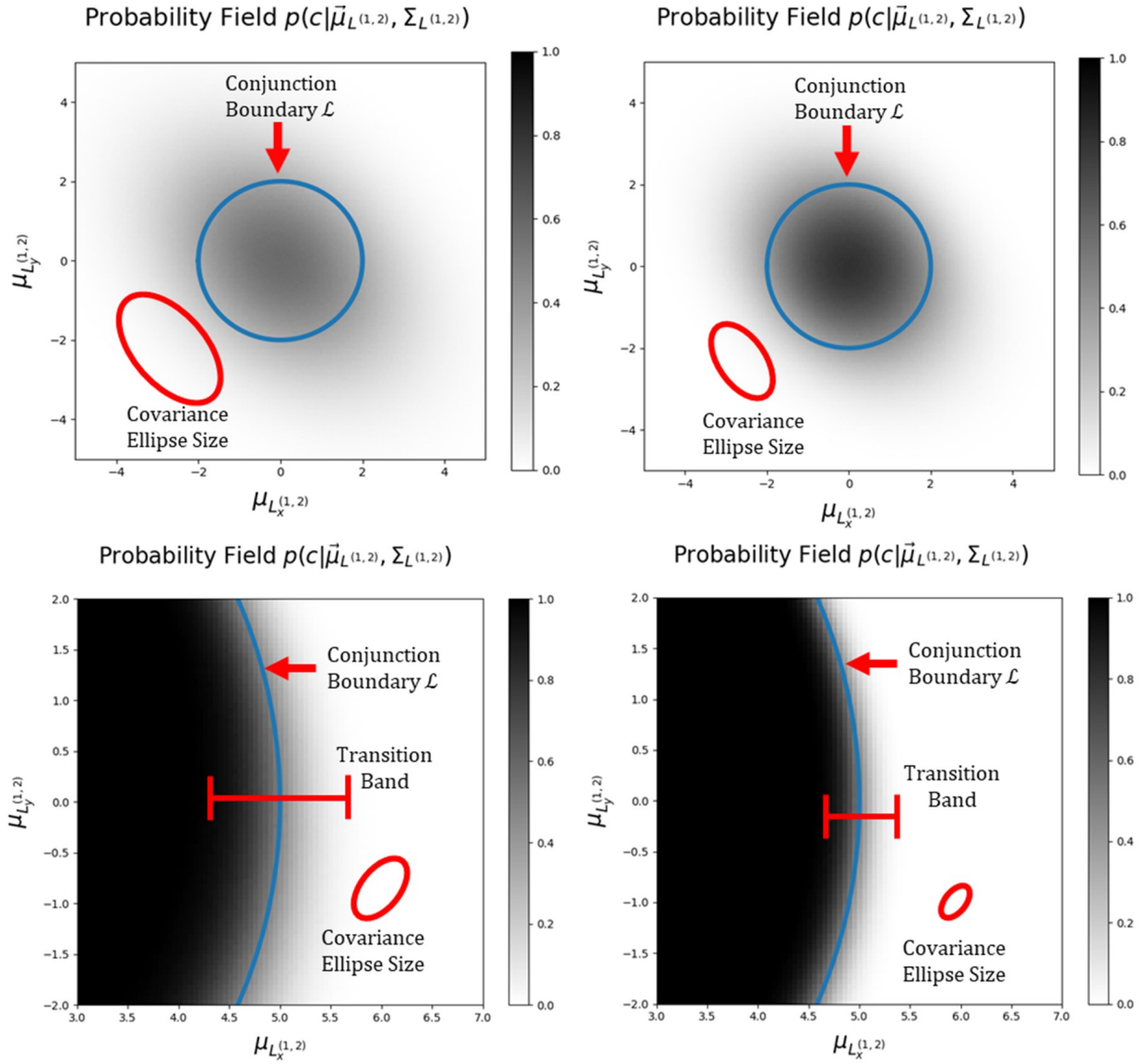

Fig. 2: A field of possible conjunction probabilities are plotted at points near the conjunction boundary. Each value in the heat map indicates a possible probability of a conjunction that could be realized if the displacement mean takes the coordinate $\vec{\mu}_{L^{(1,2)}} = \left[\mu_{L_x^{(1,2)}}, \quad \mu_{L_y^{(1,2)}} \right]^T$ and has a covariance with the size diagrammed by the red ellipse in the corresponding figure.

We find that because conjunction probability varies the most as RSOs approach their mutual conjunction boundary, it's there that the inferential variance is largest. This implies there is more to learn about trajectories that, by the nature of their approach angle, spend more time near the boundary than those that pass directly through it. This "boundary effect" for large conjunction boundaries, indicates closest-approach conjunction probability strategies may be insufficient for some cases, which corresponds to our criticism of RoT 1 in Section 2.2. Thus we find that prior and posterior covariance size and location dictates the amount of inferential variation. We will focus on these parameters in the simulation.

3.1 Simulation

We will simulate conjunction configurations, compute sensor tasking objective functions, and from these results create pairs of configurations to test the decision making of the sensor tasking schemes. We compare their ability to refine conjunction probabilities in the next subsection.

We simulated 180 conjunction configurations from combinations of the parameter values below:

Simulation Parameter	Interpretation	Relation	Values
$\mathscr{L}$	Conjunction Boundary	$\mathscr{L}$	1
α	Measurement Noise Scale	$\Sigma_Y = \Sigma_L + \alpha I$	(0.1, 0.5, 1)
β	Prior Cov Scale	$\beta\Sigma_L$	(0.01, 1 ,10)
Miss-Distance	Closest prior mean displac.	μ_{L_y}	$k(\mathscr{L} + \sigma_{L_y})$ for $k = (0, \frac{1}{4}, \frac{1}{2}, \frac{3}{4}, 1)$
Prior Cov. Shape	circular or elongated/rotated	Σ_L	(circular, horizontal, diagonal, vertical)

The simulation results are recorded in the table in Appendix 7.3. For the horizontal, diagonal, and vertical covariance shapes, one axis is set 5 times longer than the other. The miss distances varies from 0 to one standard deviation outside of the conjunction boundary $(\mathscr{L} + \sigma_{L_y})$, where σ_{L_y} is the square root of the yy component of the prior displacement covariance Σ_L. The posterior covariance is obtained using the standard Kalman Filter update with the linearized measurement function matrix H being identity: $\Sigma'_L = (I - \beta\Sigma_L(\beta\Sigma_L + \alpha I)^{-1})\beta\Sigma_L$. We depict a representative subset of the 180 conjunction configurations in Fig. 3.

For each conjunction configuration, we computed results for five candidate sensor tasking objective functions: conjunction-based inferential variance, conjunction-based Mutual Information $\mathrm{MI}[C;Y]$, closest approach conjunction probability RoT 1, trace of the posterior covariance Σ'_L RoT 2, and the custody-based Mutual Information RoT 3. The three RoT's are computed in a straight-forward manner from the configuration parameters (RoT 2 and 3) and Monte Carlo sampling for the conjunction probability at the closest approach (RoT 1). Because the conjunction-based inferential variance and the conjunction-based Mutual Information are used for optimal dynamic sensor tasking and are functions of the posterior conjunction probabilities $p(c_t^{(1,2)}|y)$, the measure variables $\rho(y)$, and prior conjunction probabilities $p(c_t^{(1,2)})$, more complex simulation is needed.

To keep the dynamics conceptually simple and generally applicable in a variety of space domains and orbital volumes, we focused on varying conjunction scenarios near and through the boundary with simple linear dynamics between the RSOs, i.e. we used prior mean displacement vectors of the form $\vec{\mu}_{L^{(1,2)}}(t) \equiv \vec{\mu}_L(t) = \begin{bmatrix}\mu_{L_x} + t v_x, & \mu_{L_y}\end{bmatrix}^T$, with μ_{L_x}, μ_{L_y} being constant initial conditions. The x spacing of evaluations is equal to the standard deviation of the smallest posterior covariance so potential boundary effects are captured. We calculate the conjunction probability at every time t, using 10^5 samples, along the trajectory. This gives us a prior distribution of conjunction probabilities $p(c_t^{(1,2)})$ for every time in the configuration. We then take $4 \cdot 10^3$ samples from $\rho(y)$ representing different possible realizations from a measurement device, which result in $4 \cdot 10^3$ different posterior horizontal trajectories, which we compute posterior conjunction probabilities $p(c_t^{(1,2)}|y)$ along, again using 10^5 samples at every time step. We use these Monte Carlo estimates to estimate conjunction-based inferential variance and Mutual Information for each time step, which we then sum over time, respectively. The summed values are recorded per configuration in the table.

Now that all five of the candidate sensor tasking objective functions have been evaluated per configuration, we create a set of $\binom{180}{2} = 16,110$ sensor tasking decision scenario pairs from the 180 different conjunction configurations. In the next section we examine the effectiveness of sensor tasking according to the five candidate methods over the set of scenarios. That is, we do the simplest form of conjunction-based sensor tasking where a single sensor (with a single observation) is forced to choose between measuring an RSO from one conjunction configuration or another.

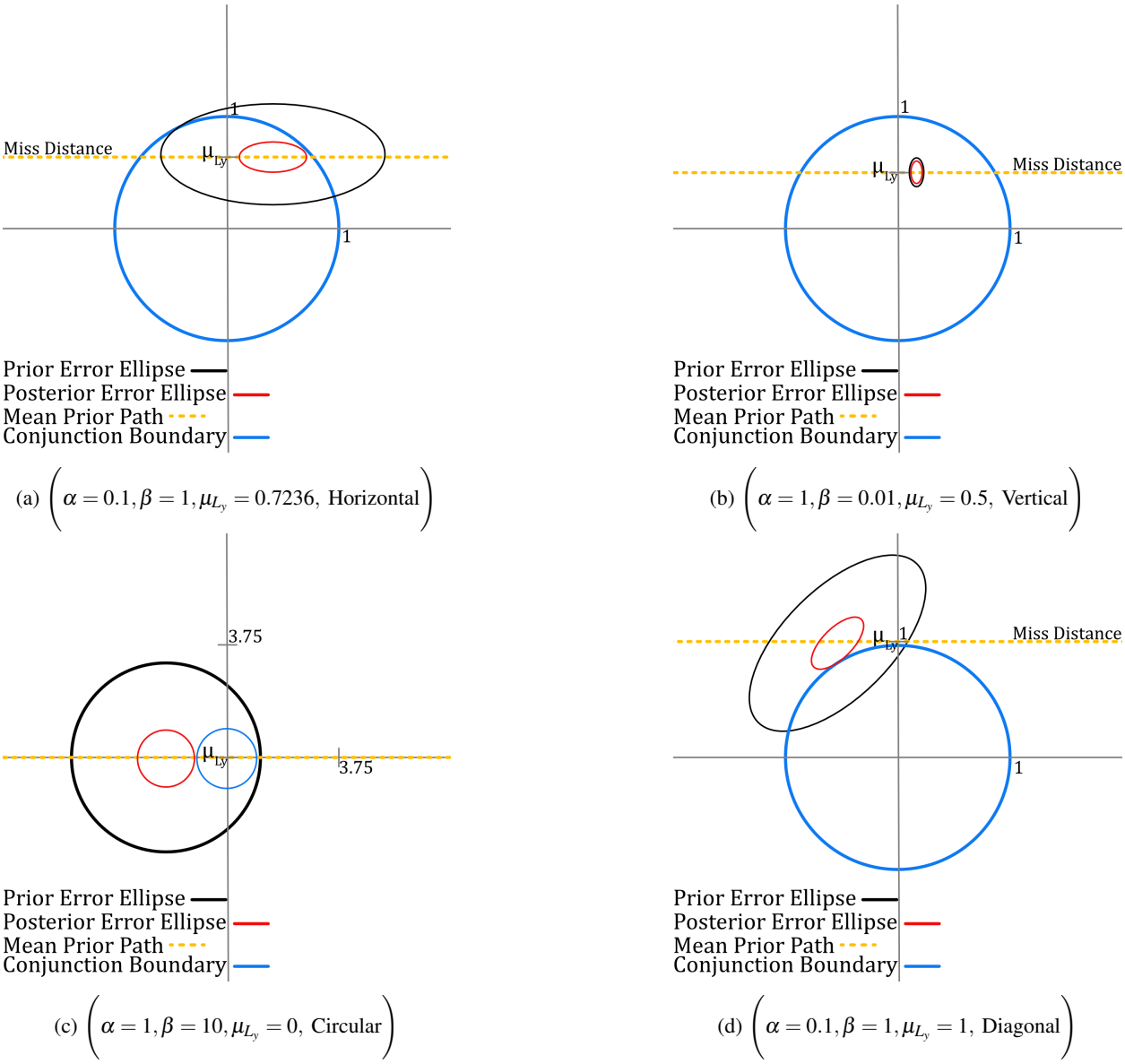

Fig. 3: Depicted are 4 of the 180 simulated conjunction configurations. Each figure notes its simulation parameters.

3.2 Results

The table below is a summary of the results of our pair-wise conjunction configuration sensor tasking experiment. Once a sensor is tasked to a configuration in the pair, the conjunction probability from the observed configuration is updated, and its mean squared error is removed. Mean squared error remains, however, for the unobserved configuration, which is the error between the current prior estimate and the possible conjunction probability posteriors that it might have been updated to if it was measured instead (i.e. measuring how well the prior approximates possible posteriors, Fig. 1 and (3)). Our method uses inferential variance to minimize the remaining mean squared error, leading to 100% of the scenarios being optimally tasked in this sense. While the conjunction-based Mutual Information performs well, at the end of the day, maximum information gain does not imply maximal error reduction. In terms of "refining probabilities" we take "epistemic probability error reduction" to be a more concrete measure of probabilistic refinement than information gain as it provides direct evidence of how much an estimate has improved.

Pair-wise Tasking Experiment	Conjunction-based IV $\max(\mathrm{Var}_Y[p(c\|y)])$ (our method)	Conjunction-based MI $\max(\mathrm{MI}[C;Y])$	Conjunct Prob. $\max(p(c\|t))$	Trace Posterior Covariance $\min(\mathrm{Tr}(\Sigma'_X))$	Custody-Based MI $\max(\mathrm{MI}[X;Y])$
Mean MSE Remaining	**0.191**	0.215	0.489	0.687	0.388
Optimally Tasked Proportion	**1**	0.881	0.579	0.382	0.643
Invariance (Failure) Modes	-	Info ≠ Error	Posterior Cov. Size	Miss-Distance	Miss-Distance

The RoT methods do not perform as well for a number of reasons. The maximum conjunction probability method is agnostic to how much a configuration would be updated by a measurement and to potential conjunction boundary effects. The last two objective functions are custody-based and thus fail to take miss distance into account, which is a crucial variable in the conjunction probability calculation. How much they improve our knowledge of the conjunction probability becomes more of a matter of chance.

We demonstrate the "small covariance boundary effect" suggested in Fig. 2 by looking at a subset of the configuration data table in Appendix 7.3. Each row in this table uses the smallest measurement scale in our simulations ($\alpha = 0.1$):

Prior Covariance Scale (β)	Miss Distance	Inferential Variance
0.01	0	0.061
0.01	0.275	0.064
0.01	0.55	0.07
0.01	**0.825**	**0.121**
0.01	1.1	0.032
1	0	1.566
1	**0.5**	**1.923**
1	1	1.584
1	1.5	0.258
1	2	0.005

Bolded are the maximum summed inferential variances along the fixed (α, β) trajectory for this set of miss distances. We plot these maximum cases relative to their zero miss distance counterparts below:

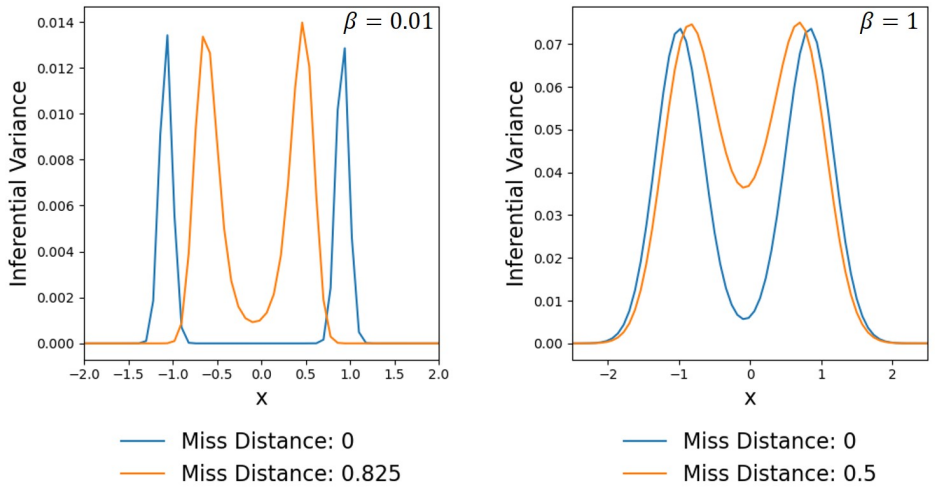

From these figures it is clear that more inferential variance can be gained or lost the longer these configurations stay "near" the conjunction boundary, where "nearness" is a function of the prior covariance. For the large $\beta = 10$ case, which has covariances that are much larger than the conjunction boundary, inferential variance is maximized for zero miss distances, i.e. the case that envelops the conjunction boundary the most.

4. CONCLUSION AND FUTURE WORK

We have demonstrated the utility and effectiveness of using inferential variance as an objective function for optimal conjunction-based sensor tasking to improve SDA. Our approach outperforms existing methods (including Mutual Information) in terms of its ability to refine conjunction probability estimates by optimally tasking sensors to directly remove the most conjunction probability estimation error. While we used this framework to solve the problem of optimally refining conjunction probability estimates, nothing in principle prevents extending this framework to other space domain scenarios beyond conjunction scenarios that might benefit from this type of targeted scenario-based optimal sensor tasking.

Exploring the concept of optimal conjunction-based sensor tasking yielded a few insights into the nature of conjunction probabilities and risk refinement. We found, while conjunction probabilities are maximal when the miss distance $\vec{\mu}_L = 0$, that the variation of conjunction probabilities is largest near the conjunction boundary $\vec{\mu}_L \approx \mathscr{L}$ instead for the large conjunction boundary case. This is to say that just because an RSO has a large conjunction probability, it doesn't mean tasking a sensor is expected to update the conjunction probability very much. This implies that "nearest approach" conjunction probability estimates may be insufficient for optimal conjunction-based sensor tasking and that considering approach and trajectory information near the boundary is useful. We found that the inferential variance may play an interesting role in *refining* expected asset risk profiles – not minimizing them – but instead for obtaining better estimates of the current risk forecast through risk weighted optimal sensor tasking, which seems new (22).

While we set up the theoretical framework for optimal multiple sensor and RSO dynamic conjunction-based sensor tasking, we only simulated optimal single sensor dynamic sensor tasking as a proof of concept. In doing so, we did not need to integrate with a full orbital propagator, consider effects of covariance non-realism [19], or worry about scalability. Further, while we proved that the inferential variance (and the Mutual Information) is a non-decreasing and supermodular objective function, due to the simplicity of our simulation scenarios, we were able to implement a brute force solution, although the problem is NP-hard in general. Future work in this space could involve taking advantage of recent work on scalable approximate algorithms for non-decreasing supermodular size constrained optimization problems of this type and perhaps combining those approaches with scalable integration methods.

5. ACKNOWLEDGEMENTS

Matt Allen, Carl Andersen, Fotis Barlos, Tony Falcone, Keshav Ganapathy, Greg Joiner, Jonathan Lasko, Alex Lay, Plamen Petrov, Kevin Schroeder, Yuri Strohm, and Aisha Yousuf

6. REFERENCES

[1] Kevin Vanslette. Inferential moments of uncertain multivariable systems. *arXiv preprint arXiv:2305.01841*, 2023.

[2] R Scott Erwin, Paul Albuquerque, Sudharman K Jayaweera, and Islam Hussein. Dynamic sensor tasking for space situational awareness. In *Proceedings of the 2010 American control conference*, pages 1153–1158. IEEE, 2010.

[3] Patrick S Williams, David B Spencer, and Richard S Erwin. Coupling of estimation and sensor tasking applied to satellite tracking. *Journal of Guidance, Control, and Dynamics*, 36(4):993–1007, 2013.

[4] Andris D Jaunzemis, Marcus J Holzinger, and K Kim Luu. Sensor tasking for spacecraft custody maintenance and anomaly detection using evidential reasoning. *Journal of Aerospace Information Systems*, 15(3):131–156, 2018.

[5] Qingli Yan and Jianfeng Chen. Sensor selection via maximizing hybrid bayesian fisher information and mutual information in unreliable sensor networks. *Electronics*, 9(2):283, 2020.

[6] Nagavenkat Adurthi, Puneet Singla, and Manoranjan Majji. Mutual information based sensor tasking with applications to space situational awareness. *Journal of Guidance, Control, and Dynamics*, 43(4):767–789, 2020.

[7] Emily Gerber, Thomas Kelecy, Bill Delude, and Bill McClintock. A consolidated multi-state orbit estimation paradigm for improved rso track custody. In *AMOS 2022 (ISSN 2576-5965)*, 2022.

[8] Peng Mun Siew, Daniel Jang, Thomas G Roberts, Richard Linares, and Justin Fletcher. Cislunar space situational awareness sensor tasking using deep reinforcement learning agents. In *AMOS 2022 (ISSN 2576-5965)*, 2022.

[9] Thomas M Cover. *Elements of information theory*. John Wiley & Sons, 1999.
[10] Nicholas Carrara and Kevin Vanslette. The design of global correlation quantifiers and continuous notions of statistical sufficiency. *Entropy*, 22(3):357, 2020.
[11] Tarunraj Singh. Optimal sensor tasking for space situational awareness. Technical Report AFRL-AFOSR-VA-TR-2020-0033, Research Foundation of State University of New York Buffalo, 2020.
[12] Chin Wa Lau, Chandra Nair, and David Ng. A mutual information inequality and some applications. *IEEE Transactions on Information Theory*, 2023.
[13] Joseph Janssen, Vincent Guan, and Elina Robeva. Ultra-marginal feature importance: Learning from data with causal guarantees. In *International Conference on Artificial Intelligence and Statistics*, pages 10782–10814. PMLR, 2023.
[14] Kiyohito Nagano, Yoshinobu Kawahara, and Kazuyuki Aihara. Size-constrained submodular minimization through minimum norm base. In *Proceedings of the 28th International Conference on Machine Learning (ICML-11)*, pages 977–984, 2011.
[15] Emma Kerr and N Sánchez Ortiz. State of the art and future needs in conjunction analysis methods, processes and software'. In *Proceedings of 8th European Conference on Space Debris (virtual edition, SDC8)*, pages 20–23, 2021.
[16] Thomas B Schön and Fredrik Lindsten. Manipulating the multivariate gaussian density. *Div. Automat. Control, Linköping Univ., Linkping, Sweden, Tech. Rep*, 4(3.4):4, 2011.
[17] Wayne W Schmaedeke. Information-based sensor management. In *Signal processing, sensor fusion, and target recognition II*, volume 1955, pages 156–164. SPIE, 1993.
[18] Islam I Hussein, Thomas Kubancik, Erin Griggs, Holly Borowski, and Mark Bolden. Risk-based decision-making for space traffic management. 2022.
[19] Jonathan Kadan, Dylan Thomas, Amit Bala, Kevin Schroeder, and Jonathan Black. Application of novel filtering approaches to modern space domain awareness. In *AMOS 2021 (ISSN 2576-5965)*, 2021.
[20] George L Nemhauser, Laurence A Wolsey, and Marshall L Fisher. An analysis of approximations for maximizing submodular set functions—i. *Mathematical programming*, 14:265–294, 1978.

7. APPENDIX

7.1 Computation of the multivariate Gaussian exhaustive inferential variance

Because the square of an exponential is the exponential with its argument doubled, the exhaustive inferential variance is exactly solvable using the following trick,

$$\begin{aligned}
\triangle(X)_Y &= \int_{x,y\in X,Y} \rho(x|y)^2\rho(y)\,dy\,dx - \int_{x\in X}\rho(x)^2\,dx \\
&= \int_{x,y\in X,Y} N\Big(\mu'_X,\Sigma'_X\Big)^2\rho(y)\,dy\,dx - \int_{x\in X} N\Big(\mu_X,\Sigma_X\Big)^2\,dx \\
&= \frac{1}{\sqrt{2}(2\pi)^{k_X/2}|\Sigma'_X|^{\frac{1}{2}}}\int_{x,y\in X,Y} N\Big(\mu'_X,\frac{\Sigma'_X}{2}\Big)\rho(y)\,dy\,dx - \frac{1}{\sqrt{2}(2\pi)^{k_X/2}|\Sigma_X|^{\frac{1}{2}}}\int_{x\in X} N\Big(\mu_X,\frac{\Sigma_X}{2}\Big)\,dx \\
&= \frac{1}{\sqrt{2}(2\pi)^{k_X/2}}\Big(\frac{1}{|\Sigma'_X|^{\frac{1}{2}}} - \frac{1}{|\Sigma_X|^{\frac{1}{2}}}\Big) \qquad (23)\\
&= \frac{1}{\sqrt{2}(2\pi)^{k_X/2}}\Big(\frac{1}{|\Sigma_X - \Sigma_{XY}^T\Sigma_Y^{-1}\Sigma_{XY}|^{\frac{1}{2}}} - \frac{1}{|\Sigma_X|^{\frac{1}{2}}}\Big) \\
&= \frac{1}{\sqrt{2}(2\pi)^{k_X/2}}\Big(\frac{|\Sigma_Y|^{\frac{1}{2}}}{|\Sigma_Z|^{\frac{1}{2}}} - \frac{1}{|\Sigma_X|^{\frac{1}{2}}}\Big), \qquad (24)
\end{aligned}$$

where equation (23) is true due to normalization and equation (24) used the block matrix determinant identity $|\Sigma_Z| = |\Sigma_Y||\Sigma_X - \Sigma_{XY}^T\Sigma_Y^{-1}\Sigma_{XY}|$.

7.2 Non-Decreasing and Supermodular Proofs

Definitions of a non-decreasing and supermodular set function are provided by [20]. We use the following definition of a non-decreasing function,

$$f(C) \geq f(A), \tag{25}$$

where $A \subset C \subset E$. Further, we use the following definition of a supermodular function (negative of the submodular definition),

$$\triangle_e(C) \geq \triangle_e(A) \tag{26}$$

again where $A \subset C \subset E$ but where $e \in E - B$, and where, for any S,

$$\triangle_e(S) = f(S \cup \{e\}) - f(S). \tag{27}$$

We will deviate from previous notation in this section for simplicity by letting Y_S be the joint variable space of the sensors in S and $y_S \in Y_S$.

7.2.1 Inferential Variance and Exhaustive Inferential Variance

Because the exhaustive inferential variance is a sum of inferential variances, we only need to prove the inferential variance is non-decreasing and supermodular because the sum of non-decreasing supermodular functions is non-decreasing supermodular. For this proof and the next, we will use the following variance decomposition relationship from [1],

$$\mathrm{Var}_{Y_A,Y_B}\Big[\rho(x|y_A,y_B)\Big] \quad = \quad \mathrm{E}_{Y_B}\left[\mathrm{Var}_{Y_A}\Big[\rho(x|y_A,y_B)\Big|y_B\Big]\right] + \mathrm{Var}_{Y_A}\Big[\rho(x|y_A)\Big], \tag{28}$$

which is the expected posterior inferential variance (due to an unknown measurement from Y_B) plus the partial inferential variance.

We now prove the inferential variance is non-decreasing. Working with the variables of a single RSO (x), let A, B, C be sets of sensors such that $A \cap B = \emptyset$ and $C = A \cup B$ such that $A \subset C$ and let

$$f_{IV}(S) \equiv \mathrm{Var}_{Y_S}\Big[\rho(x|y_S)\Big].$$

Because variances and expected variances are non-negative, the inferential variance is non-decreasing,

$$f_{IV}(C) = \mathrm{Var}_{Y_C}\Big[\rho(x|y_C)\Big] = \mathrm{Var}_{Y_A,Y_B}\Big[\rho(x|y_A,y_B)\Big] \geq \mathrm{Var}_{Y_A}\Big[\rho(x|y_A)\Big] = f_{IV}(A), \tag{29}$$

where we used (28) and definition (26). Note that while we used the variables x and y, the relations hold in general for the inferential variance of any quantities.

We now prove the inferential variance is supermodular. Let $S_e = S \cup \{e\}$. Because the variance for three variables can be decomposed as,

$$f_{IV}(C_e) = \mathrm{Var}_{Y_A,Y_e,Y_B}\Big[\rho(x|y_A,y_e,y_B)\Big] \quad = \quad \mathrm{E}_{Y_B}\left[\mathrm{Var}_{Y_AY_e}\Big[\rho(x|y_A,y_e,y_B)\Big|y_B\Big]\right] + \mathrm{Var}_{Y_AY_e}\Big[\rho(x|y_A,y_e)\Big], \tag{30}$$

and,

$$f_{IV}(C) = \mathrm{Var}_{Y_A,Y_B}\Big[\rho(x|y_A,y_B)\Big] \quad = \quad \mathrm{E}_{Y_B}\left[\mathrm{Var}_{Y_A}\Big[\rho(x|y_A,y_B)\Big|y_B\Big]\right] + \mathrm{Var}_{Y_A}\Big[\rho(x|y_A)\Big], \tag{31}$$

we have,

$$\triangle_e(C) = f_{IV}(C_e) - f_{IV}(C) = \mathrm{E}_{Y_B}\left[\mathrm{Var}_{Y_A,Y_e}\Big[\rho(x|y_A,y_e,y_B)\Big|y_B\Big]\right] - \mathrm{E}_{Y_B}\left[\mathrm{Var}_{Y_A}\Big[\rho(x|y_A,y_B)\Big|y_B\Big]\right] + \triangle_e(A) \geq \triangle_e(A), \tag{32}$$

proving supermodularity. The inequality is due to the non-negativity of

$$\begin{aligned}&\mathrm{E}_{Y_B}\left[\mathrm{Var}_{Y_A,Y_e}\left[\rho(x|y_A,y_e,y_B)\Big|y_B\right]\right]-\mathrm{E}_{Y_B}\left[\mathrm{Var}_{Y_A}\left[\rho(x|y_A,y_B)\Big|y_B\right]\right]\\&=\mathrm{E}_{Y_B}\left[\mathrm{Var}_{Y_A,Y_e}\left[\rho(x|y_A,y_e,y_B)\Big|y_B\right]-\mathrm{Var}_{Y_A}\left[\rho(x|y_A,y_B)\Big|y_B\right]\right],\end{aligned}\tag{33}$$

because every term in the expectation value is non-negative,

$$\mathrm{Var}_{Y_A,Y_e}\left[\rho(x|y_A,y_e,y_B)\Big|y_B\right]\geq\mathrm{Var}_{Y_A}\left[\rho(x|y_A,y_B)\Big|y_B\right]\tag{34}$$

again due to (28) or the non-decreasing property of the inferential variance (both hold for the conditional variance as well). Thus, the inferential variance, and by extension the exhaustive inferential variance, are in general non-decreasing and supermodular.

7.2.2 Mutual Information (MI)

We provide a proof the MI is non-decreasing and supermodular (modeled after the strategy used in [12, 13], but yielding results contrary to [6]), in the sensor tasking framework. We use the following relations: let

$$f_{MI}(S)\equiv\mathrm{MI}[X;Y]=\int_{y\in Y}\int_{x\in X}\rho(x,y)\ln\Big(\frac{\rho(x,y)}{\rho(x)\rho(y)}\Big)\,dxdy\geq 0,$$

be the MI. The MI is symmetric $\mathrm{MI}[X;Y]=\mathrm{MI}[Y;X]$ and has a chain rule:

$$\mathrm{MI}[X;Y,Z]=\mathrm{MI}[X;Y]+\mathrm{MI}[X;Z|Y]=\mathrm{MI}[X;Z]+\mathrm{MI}[X;Y|Z]\tag{35}$$

where

$$\mathrm{MI}[X;Y|Z]=\int_{z\in Z}\rho(z)\left(\int_{y\in Y}\int_{x\in X}\rho(x,y|z)\ln\Big(\frac{\rho(x,y|z)}{\rho(x|z)\rho(y|z)}\Big)\,dxdy\right)dz\geq 0,\tag{36}$$

is the conditional MI.

The chain rule implies the MI is non-decreasing as new sensors are added to measure X,

$$\begin{aligned}f_{MI}(C)&=\mathrm{MI}[X;Y_C]=\mathrm{MI}[X;Y_A,Y_B]=\mathrm{MI}[X;Y_A]+\mathrm{MI}[X;Y_B|Y_A]\\&\geq\mathrm{MI}[X;Y_A]=f_{MI}(A),\end{aligned}\tag{37}$$

which is definition (25).

The proof of supermodularity is done under the assumption that, given the of the knowledge of X, that sensors are conditionally independent of one another, i.e. $\rho(y_A,y_B,y_e|x)=\rho(y_A|x)\rho(y_B|x)\rho(y_e|x)$. This assumption is equally used in [6]. The validity of the assumption is apparent from the form of the measurement equations in the Kalman Filter paradigm $y^{(k)}=\theta^{(m,k)}(h(x^{(m)})+\omega^{(m,k)})$. The $y^{(k)}$ does not have dependence on other $y^{(k')}$, given $x^{(m)}$, which is a statement of the conditional independence of sensors.

We now prove the supermodularity of the MI under conditionally independent sensor variables. First note

$$\begin{aligned}\triangle_e(A)&=f_{MI}(A_e)-f_{MI}(A)\\&=\mathrm{MI}[X;Y_A,Y_e]-\mathrm{MI}[X;Y_A]\\&=\mathrm{MI}[X;Y_A]+\mathrm{MI}[X;Y_e|Y_A]-\mathrm{MI}[X;Y_A]\quad\text{(chain)}\\&=\mathrm{MI}[X;Y_e|Y_A]=\mathrm{MI}[Y_e;X|Y_A]\quad\text{(symmetry)}\\&=\mathrm{MI}[Y_e;X,Y_A]-\mathrm{MI}[Y_e;Y_A]\quad\text{(chain)}\end{aligned}\tag{38}$$

and

$$\begin{aligned}
\triangle_e(C) &= f_{MI}(C_e) - f_{MI}(C) \\
&= \mathrm{MI}[X;Y_A,Y_e,Y_B] - \mathrm{MI}[X;Y_A,Y_B] \\
&= \mathrm{MI}[X;Y_A,Y_B] + \mathrm{MI}[X;Y_e|Y_A,Y_B] - \mathrm{MI}[X;Y_A,Y_B] \quad \text{(chain)} \\
&= \mathrm{MI}[X;Y_e|Y_A,Y_B] = \mathrm{MI}[Y_e;X|Y_A,Y_B] \quad \text{(symmetry)} \\
&= \mathrm{MI}[Y_e;X,Y_A,Y_B] - \mathrm{MI}[Y_e;Y_A,Y_B] \quad \text{(chain)} \qquad (39)
\end{aligned}$$

is the same form. Continuing on $\triangle_e(C)$ and doing the chain rule on both terms,

$$\begin{aligned}
\triangle_e(C) &= \Big(\mathrm{MI}[Y_e;X,Y_A]) - \mathrm{MI}[Y_e;Y_B|X,Y_A])\Big) - \Big(\mathrm{MI}[Y_e;Y_A] - \mathrm{MI}[Y_e;Y_B|Y_A]\Big) \quad \text{(chains)} \\
&= \mathrm{MI}[Y_e;Y_B|Y_A]) + \mathrm{MI}[Y_e;X,Y_A]) - \mathrm{MI}[Y_e;Y_A] \quad \text{(conditional independence)} \\
&= \mathrm{MI}[Y_e;Y_B|Y_A]) + \triangle_e(A) \geq \triangle_e(A), \qquad (40)
\end{aligned}$$

which is definition (26). For the conditional independence step, we used

$$\begin{aligned}
\mathrm{MI}[Y_e;Y_B|X,Y_A] &= \int_{y_A\in Y_A}\int_{x\in X}\rho(x,y_A)\left(\int_{y_e\in Y_e}\int_{y_B\in Y_B}\rho(y_e,y_B|x,y_A)\ln\left(\frac{\rho(y_e,y_B|x,y_A)}{\rho(y_e|x,y_A)\rho(y_B|x,y_A)}\right)dy_e\,dy_B\right)dy_A\,dx \\
&= \int_{y_A\in Y_A}\int_{x\in X}\rho(x,y_A)\left(\int_{y_e\in Y_e}\int_{y_B\in Y_B}\rho(y_e|x)\rho(y_B|x)\ln\left(\frac{\rho(y_e|x)\rho(y_B|x)}{\rho(y_e|x)\rho(y_B|x)}\right)dy_e\,dy_B\right)dy_A\,dx \\
&= 0 \qquad (41)
\end{aligned}$$

which is due to $\rho(y_e,y_B|x,y_A) = \rho(y_e|x,y_A)\rho(y_B|x,y_A,y_e) = \rho(y_B|x)\rho(y_e|x)$. Further, it should be noted that $\mathrm{MI}[Y_e;Y_B|Y_A] \geq 0$ because conditional independence does not imply marginal independence as $\int_{x\in X}\rho(x)\rho(y_A|x)\rho(y_B|x)\rho(y_e|x)\,dx \neq \rho(y_A)\rho(y_B)\rho(y_e)$ in general. Thus, the MI is supermodular in terms of the number of conditionally independent sensors tasked to measure an RSO. These relations hold trivially for multi-RSO dynamical systems $X \to \mathbb{X}_{0:\tau}$ and as well supermodularity extends to sums of MIs that might appear in a MI-based sensor tasking scheme.

7.3 Simulated Conjunction Configurations

Measurement Scale (α)	Prior Cov. Scale (β)	Miss Distance	Cov. Type	Inferential Variance	Conj.-based MI	Close. Appr. Conj. Prob. (RoT 1)	Trace of Posterior (RoT 2)	Custody-based MI (RoT 3)
0.1	0.01	0	Circular	0.061	0.098	1	0.018	0.095
0.1	0.01	0.275	Circular	0.064	0.102	1	0.018	0.095
0.1	0.01	0.55	Circular	0.07	0.11	1	0.018	0.095
0.1	0.01	0.825	Circular	0.121	0.168	0.954	0.018	0.095
0.1	0.01	1.1	Circular	0.032	0.159	0.148	0.018	0.095
0.5	0.01	0	Circular	0.013	0.021	1	0.02	0.02
0.5	0.01	0.275	Circular	0.014	0.022	1	0.02	0.02
0.5	0.01	0.55	Circular	0.016	0.025	1	0.02	0.02
0.5	0.01	0.825	Circular	0.027	0.037	0.954	0.02	0.02
0.5	0.01	1.1	Circular	0.007	0.036	0.146	0.02	0.02
1	0.01	0	Circular	0.007	0.011	1	0.02	0.01
1	0.01	0.275	Circular	0.007	0.011	1	0.02	0.01
1	0.01	0.55	Circular	0.009	0.013	1	0.02	0.01
1	0.01	0.825	Circular	0.013	0.019	0.955	0.02	0.01
1	0.01	1.1	Circular	0.003	0.018	0.146	0.02	0.01
0.1	1	0	Circular	1.57	2.51	0.947	0.182	2.4
0.1	1	0.5	Circular	1.92	2.98	0.813	0.182	2.4
0.1	1	1	Circular	1.58	3.31	0.42	0.182	2.4

0.1	1	1.5	Circular	0.258	1.54	0.085	0.182	2.4
0.1	1	2	Circular	0.005	0.176	0.005	0.182	2.4
0.5	1	0	Circular	1.47	3.08	0.593	0.667	1.1
0.5	1	0.5	Circular	1.5	3.24	0.52	0.667	1.1
0.5	1	1	Circular	1.22	3.26	0.331	0.667	1.1
0.5	1	1.5	Circular	0.614	2.64	0.163	0.667	1.1
0.5	1	2	Circular	0.157	1.39	0.054	0.667	1.1
1	1	0	Circular	0.971	2.47	0.486	1	0.693
1	1	0.5	Circular	0.985	2.53	0.435	1	0.693
1	1	1	Circular	0.905	2.74	0.306	1	0.693
1	1	1.5	Circular	0.511	2.31	0.165	1	0.693
1	1	2	Circular	0.177	1.48	0.069	1	0.693
0.1	10	0	Circular	1.8	2.91	0.919	0.198	4.62
0.1	10	1.04	Circular	1.52	3.43	0.373	0.198	4.62
0.1	10	2.08	Circular	0.007	0.208	0.005	0.198	4.62
0.1	10	3.12	Circular	2.20E-8	1.12E-4	1.17E-6	0.198	4.62
0.1	10	4.16	Circular	0	0	0	0.198	4.62
0.5	10	0	Circular	1.51	4.07	0.418	0.952	3.04
0.5	10	1.04	Circular	1.3	4.27	0.265	0.952	3.04
0.5	10	2.08	Circular	0.322	2.37	0.069	0.952	3.04
0.5	10	3.12	Circular	0.013	0.43	0.006	0.952	3.04
0.5	10	4.16	Circular	1.97E-4	0.033	2.46E-4	0.952	3.04
1	10	0	Circular	0.857	3.67	0.25	1.82	2.4
1	10	1.04	Circular	0.769	3.66	0.193	1.82	2.4
1	10	2.08	Circular	0.391	2.97	0.087	1.82	2.4
1	10	3.12	Circular	0.074	1.3	0.022	1.82	2.4
1	10	4.16	Circular	0.005	0.29	0.003	1.82	2.4
0.1	0.01	0	Horizontal	0.061	0.097	1	0.011	0.095
0.1	0.01	0.261	Horizontal	0.062	0.099	1	0.011	0.095
0.1	0.01	0.522	Horizontal	0.061	0.098	1	0.011	0.095
0.1	0.01	0.784	Horizontal	0.07	0.111	1	0.011	0.095
0.1	0.01	1.04	Horizontal	0.02	0.111	0.136	0.011	0.095
0.5	0.01	0	Horizontal	0.014	0.022	1	0.012	0.02
0.5	0.01	0.261	Horizontal	0.014	0.022	1	0.012	0.02
0.5	0.01	0.522	Horizontal	0.014	0.022	1	0.012	0.02
0.5	0.01	0.784	Horizontal	0.015	0.024	1	0.012	0.02
0.5	0.01	1.04	Horizontal	0.004	0.026	0.135	0.012	0.02
1	0.01	0	Horizontal	0.007	0.011	1	0.012	0.01
1	0.01	0.261	Horizontal	0.007	0.011	1	0.012	0.01
1	0.01	0.522	Horizontal	0.007	0.012	1	0.012	0.01
1	0.01	0.784	Horizontal	0.008	0.013	1	0.012	0.01
1	0.01	1.04	Horizontal	0.002	0.013	0.136	0.012	0.01
0.1	1	0	Horizontal	1.64	2.63	0.98	0.109	2.4
0.1	1	0.362	Horizontal	1.64	2.65	0.966	0.109	2.4
0.1	1	0.724	Horizontal	1.75	2.85	0.804	0.109	2.4
0.1	1	1.08	Horizontal	0.692	2.29	0.215	0.109	2.4
0.1	1	1.45	Horizontal	0.004	0.141	0.004	0.109	2.4
0.5	1	0	Horizontal	2.04	3.58	0.786	0.4	1.1
0.5	1	0.362	Horizontal	1.94	3.5	0.73	0.4	1.1
0.5	1	0.724	Horizontal	1.67	3.51	0.516	0.4	1.1
0.5	1	1.08	Horizontal	0.79	2.8	0.218	0.4	1.1
0.5	1	1.45	Horizontal	0.099	1.1	0.043	0.4	1.1
1	1	0	Horizontal	1.6	3.08	0.704	0.6	0.693
1	1	0.362	Horizontal	1.55	3.09	0.642	0.6	0.693

1	1	0.724	Horizontal	1.31	3.04	0.453	0.6	0.693
1	1	1.08	Horizontal	0.656	2.47	0.213	0.6	0.693
1	1	1.45	Horizontal	0.109	1.14	0.054	0.6	0.693
0.1	10	0	Horizontal	1.82	2.94	0.972	0.119	4.62
0.1	10	0.604	Horizontal	1.9	3.06	0.87	0.119	4.62
0.1	10	1.21	Horizontal	0.253	1.51	0.086	0.119	4.62
0.1	10	1.81	Horizontal	3.33E-7	6.20E-4	7.65E-6	0.119	4.62
0.1	10	2.41	Horizontal	0	0	0	0.119	4.62
0.5	10	0	Horizontal	2.63	5.29	0.636	0.571	3.04
0.5	10	0.604	Horizontal	2.26	5.09	0.479	0.571	3.04
0.5	10	1.21	Horizontal	0.786	3.55	0.149	0.571	3.04
0.5	10	1.81	Horizontal	0.024	0.604	0.011	0.571	3.04
0.5	10	2.41	Horizontal	8.10E-5	0.019	1.70E-04	0.571	3.04
1	10	0	Horizontal	2.06	5.55	0.442	1.09	2.4
1	10	0.604	Horizontal	1.77	5.29	0.343	1.09	2.4
1	10	1.21	Horizontal	0.803	4.08	0.141	1.09	2.4
1	10	1.81	Horizontal	0.124	1.69	0.031	1.09	2.4
1	10	2.41	Horizontal	0.004	0.224	0.002	1.09	2.4
0.1	0.01	0	Vertical	0.027	0.043	1	0.011	0.095
0.1	0.01	0.275	Vertical	0.033	0.052	1	0.011	0.095
0.1	0.01	0.55	Vertical	0.049	0.072	1	0.011	0.095
0.1	0.01	0.825	Vertical	0.102	0.133	0.959	0.011	0.095
0.1	0.01	1.1	Vertical	0.031	0.146	0.152	0.011	0.095
0.5	0.01	0	Vertical	0.006	0.009	1	0.012	0.02
0.5	0.01	0.275	Vertical	0.007	0.012	1	0.012	0.02
0.5	0.01	0.55	Vertical	0.011	0.016	1	0.012	0.02
0.5	0.01	0.825	Vertical	0.023	0.03	0.958	0.012	0.02
0.5	0.01	1.1	Vertical	0.007	0.033	0.156	0.012	0.02
1	0.01	0	Vertical	0.003	0.005	1	0.012	0.01
1	0.01	0.275	Vertical	0.004	0.006	1	0.012	0.01
1	0.01	0.55	Vertical	0.006	0.008	1	0.012	0.01
1	0.01	0.825	Vertical	0.012	0.015	0.958	0.012	0.01
1	0.01	1.1	Vertical	0.004	0.017	0.156	0.012	0.01
0.1	1	0	Vertical	0.746	1.15	0.981	0.109	2.4
0.1	1	0.5	Vertical	1.31	1.7	0.881	0.109	2.4
0.1	1	1	Vertical	1.52	2.62	0.489	0.109	2.4
0.1	1	1.5	Vertical	0.299	1.42	0.107	0.109	2.4
0.1	1	2	Vertical	0.009	0.209	0.008	0.109	2.4
0.5	1	0	Vertical	0.936	1.55	0.788	0.4	1.1
0.5	1	0.5	Vertical	1.19	1.88	0.697	0.4	1.1
0.5	1	1	Vertical	1.32	2.49	0.46	0.4	1.1
0.5	1	1.5	Vertical	0.742	2.23	0.232	0.4	1.1
0.5	1	2	Vertical	0.183	1.22	0.076	0.4	1.1
1	1	0	Vertical	0.746	1.38	0.7	0.6	0.693
1	1	0.5	Vertical	0.906	1.59	0.628	0.6	0.693
1	1	1	Vertical	0.999	2.02	0.441	0.6	0.693
1	1	1.5	Vertical	0.655	1.94	0.247	0.6	0.693
1	1	2	Vertical	0.246	1.35	0.105	0.6	0.693
0.1	10	0	Vertical	0.882	1.35	0.972	0.119	4.62
0.1	10	1.04	Vertical	1.58	2.89	0.448	0.119	4.62
0.1	10	2.08	Vertical	0.008	0.196	0.007	0.119	4.62
0.1	10	3.12	Vertical	1.37E-9	2.44E-5	3.85E-7	0.119	4.62
0.1	10	4.16	Vertical	0	0	0	0.119	4.62
0.5	10	0	Vertical	1.28	2.43	0.63	0.571	3.04

0.5	10	1.04	Vertical	1.46	3.21	0.41	0.571	3.04
0.5	10	2.08	Vertical	0.419	2.07	0.109	0.571	3.04
0.5	10	3.12	Vertical	0.022	0.43	0.011	0.571	3.04
0.5	10	4.16	Vertical	1.44E-04	0.025	4.04E-04	0.571	3.04
1	10	0	Vertical	0.988	2.55	0.44	1.09	2.4
1	10	1.04	Vertical	0.995	2.82	0.338	1.09	2.4
1	10	2.08	Vertical	0.59	2.59	0.156	1.09	2.4
1	10	3.12	Vertical	0.129	1.28	0.041	1.09	2.4
1	10	4.16	Vertical	0.008	0.273	0.006	1.09	2.4
0.1	0.01	0	Diagonal	0.028	0.044	1	0.011	0.095
0.1	0.01	0.275	Diagonal	0.032	0.05	1	0.011	0.095
0.1	0.01	0.55	Diagonal	0.047	0.07	1	0.011	0.095
0.1	0.01	0.825	Diagonal	0.104	0.135	0.958	0.011	0.095
0.1	0.01	1.1	Diagonal	0.029	0.139	0.152	0.011	0.095
0.5	0.01	0	Diagonal	0.006	0.01	1	0.012	0.02
0.5	0.01	0.275	Diagonal	0.007	0.012	1	0.012	0.02
0.5	0.01	0.55	Diagonal	0.011	0.017	1	0.012	0.02
0.5	0.01	0.825	Diagonal	0.022	0.029	0.958	0.012	0.02
0.5	0.01	1.1	Diagonal	0.007	0.034	0.153	0.012	0.02
1	0.01	0	Diagonal	0.003	0.005	1	0.012	0.01
1	0.01	0.275	Diagonal	0.004	0.006	1	0.012	0.01
1	0.01	0.55	Diagonal	0.006	0.008	1	0.012	0.01
1	0.01	0.825	Diagonal	0.012	0.016	0.959	0.012	0.01
1	0.01	1.1	Diagonal	0.003	0.017	0.153	0.012	0.01
0.1	1	0	Diagonal	0.774	1.19	0.981	0.11	2.4
0.1	1	0.502	Diagonal	1.38	1.81	0.87	0.11	2.4
0.1	1	1	Diagonal	1.51	2.64	0.479	0.11	2.4
0.1	1	1.5	Diagonal	0.267	1.32	0.107	0.11	2.4
0.1	1	2.01	Diagonal	0.009	0.203	0.008	0.11	2.4
0.5	1	0	Diagonal	0.961	1.61	0.785	0.405	1.1
0.5	1	0.502	Diagonal	1.24	1.95	0.688	0.405	1.1
0.5	1	1	Diagonal	1.34	2.51	0.47	0.405	1.1
0.5	1	1.5	Diagonal	0.738	2.23	0.228	0.405	1.1
0.5	1	2.01	Diagonal	0.19	1.24	0.074	0.405	1.1
1	1	0	Diagonal	0.719	1.34	0.697	0.608	0.693
1	1	0.502	Diagonal	0.888	1.58	0.621	0.608	0.693
1	1	1	Diagonal	0.969	1.97	0.445	0.608	0.693
1	1	1.5	Diagonal	0.62	1.87	0.244	0.608	0.693
1	1	2.01	Diagonal	0.234	1.29	0.107	0.608	0.693
0.1	10	0	Diagonal	0.881	1.35	0.972	0.12	4.62
0.1	10	1.05	Diagonal	1.49	2.79	0.433	0.12	4.62
0.1	10	2.09	Diagonal	0.01	0.218	0.007	0.12	4.62
0.1	10	3.14	Diagonal	3.14E-9	3.62E-5	5.80E-7	0.12	4.62
0.1	10	4.18	Diagonal	0	0	0	0.12	4.62
0.5	10	0	Diagonal	1.28	2.42	0.633	0.579	3.04
0.5	10	1.05	Diagonal	1.43	3.14	0.41	0.579	3.04
0.5	10	2.09	Diagonal	0.423	2.11	0.108	0.579	3.04
0.5	10	3.14	Diagonal	0.02	0.401	0.01	0.579	3.04
0.5	10	4.18	Diagonal	7.41E-5	0.02	3.23E-4	0.579	3.04
1	10	0	Diagonal	0.944	2.47	0.438	1.1	2.4
1	10	1.05	Diagonal	0.999	2.9	0.329	1.1	2.4
1	10	2.09	Diagonal	0.556	2.52	0.148	1.1	2.4
1	10	3.14	Diagonal	0.115	1.2	0.038	1.1	2.4
1	10	4.18	Diagonal	0.008	0.265	0.005	1.1	2.4